JOURNAL OF SOLID STATE CHEMISTRY **132,** 355–360 (1997)
ARTICLE NO. SC977474

Structure of ZrV_2O_7 from −263 to 470°C

N. Khosrovani and A. W. Sleight[1]

Department of Chemistry, Oregon State University, Corvallis, Oregon 97331

and

T. Vogt

Physics Department, Brookhaven National Laboratory, Upton, Long Island, New York 11973

Received January 21, 1997; in revised form May 6, 1997; accepted May 13, 1997

High-resolution neutron powder diffraction data were used to analyze the structure of ZrV_2O_7 at seven temperatures from −263 to 470°C. The structure of ZrV_2O_7 at 236°C was also refined using X-ray powder diffraction data. The thermal expansion is positive below about 100°C but becomes strongly negative above this temperature. Data from 88 to 470°C were refined using a 8.8 Å cubic $Z = 4$ cell in space group $Pa\bar{3}$. All V–O–V angles are 180° on average in this structure. Data from −263 to 66°C were refined with a 26.3 Å, $Z = 108$ cell still in space group $Pa\bar{3}$. 89% of the V–O–V linkages are bent to about 160° but 11% remain on three-fold axes and are therefore constrained by symmetry to be 180° on average. The strong negative thermal expansion of ZrV_2O_7 above 100°C is attributed to the transverse thermal motion of oxygen atoms in the metal–oxygen–metal linkages. These thermal motions can occur only by changing the shape of the polyhedra; thus, the occurrence of negative thermal expansion for cubic AM_2O_7 compounds is strongly correlated with the rigidity of the AO_6 octahedra and MO_4 tetrahedra.

INTRODUCTION

ZrV_2O_7 and HfV_2O_7 have been of interest because of their strong negative thermal expansion from about 100°C to about 800°C (1, 2). This is especially interesting because the contraction is isotropic due to the cubic structure of these compounds. First-order phase transitions occur for ZrV_2O_7 and HfV_2O_7 at about 77 and 100°C (1, 2). Below 77°C, these phases still appear to be cubic, but a $3 \times 3 \times 3$ superstructure has developed (2). The situation between the two phase transitions has been unclear.

We present a study of the structure of ZrV_2O_7 based on high-resolution neutron powder diffraction data. Data were obtained over a wide temperature range above and below the phase transitions. The scattering amplitude for neutrons is very low for vanadium. However, our primary interest in this structure was in the positions and thermal motions of oxygen atoms, and these might be better determined with neutron data than with X-ray data.

EXPERIMENTAL

Our synthesis of ZrV_2O_7 has been previously described (2). Neutron diffraction data were collected at the high-resolution neutron powder diffractometer at beam line H1A of the high-flux beam reactor at Brookhaven National Laboratory. Details of this instrument may be found elsewhere (3). X-ray diffraction data at 236°C were collected on a Siemens D5000 diffractometer using Cu$K\alpha$ radiation. Rietveld refinements on both the X-ray and neutron data used the GSAS software (4). A small amount of V_2O_5 was present in our sample, and neutron data above room temperature also contained peaks of aluminum due to furnace heat shields. Thus, refinements were either 2-phase or 3-phase refinements.

RESULTS

High-Temperature Structure

Data collected at 88, 114, 236, and 470°C were refined in space group $Pa\bar{3}$ with $Z = 4$. Cell edges and agreement factors are given in Table 1, and examples of observed and calculated patterns are given in Fig. 1. Refined parameters are in Table 2, and bond distances and angles are given in Table 3.

[1] To whom correspondence should be addressed.

0022-4596/97 $25.00

TABLE 1
Cell Parameters and Agreement Factors at Different Temperatures

	88°C	114°C	236°C[a]	470°C
a (Å)[b]	8.8032(1)	8.8194(1)	8.8188(1)	8.7987(1)
R_{wp}[c]	0.0667	0.0593	0.1518	0.0420
$R(F)$[d]	0.0600	0.0432	0.0607	0.0522
$R(F^2)$[e]	0.0702	0.0538	0.0927	0.0590
χ^2[f]	0.6262	0.4996	3.067	0.3368

[a] X-ray diffraction data.
[b] Standard deviation in parentheses are those calculated by GSAS. Considering the uncertainties in the wavelength and temperature, the uncertainty of the cell edges would be much larger.

[c] $R_{wp} = \dfrac{\sum w_i [y_i(\text{obs}) - y_i(\text{calc})]^2}{\sum w_i [y_i(\text{obs})]^2}$.

[d] $R(F) = \dfrac{\sum |[I(\text{obs})]^{1/2} - [I(\text{calc})]^{1/2}|}{\sum [I(\text{obs})]^{1/2}}$.

[e] $R(F^2) = \dfrac{\sum |I(\text{obs}) - I(\text{calc})|}{\sum I(\text{obs})}$.

[f] $\chi^2 = \dfrac{\sum w_i [y_i(\text{obs}) - y_i(\text{calc})]^2}{N(\text{obs}) - N(\text{var})}$.

TABLE 2
Fractional Coordinates and Thermal Parameters at Different Temperatures with Standard Deviations in Parentheses

Atom		88°C	114°C	236°C	470°C
Zr	x	0	0	0	0
	U(iso)	0.0237(7)	0.0215(6)	0.0039(4)	0.0282(5)
V	x	0.3817(36)	0.3865(23)	0.3884(2)	0.3827(23)
	U(iso)	0.0156(125)	0.0000(0)[a]	0.0058(6)	0.0169(68)
O1	x	0.4363(3)	0.4366(3)	0.4387(5)	0.4371(2)
	y	0.2058(2)	0.2052(2)	0.2086(4)	0.2056(2)
	z	0.4070(3)	0.4072(3)	0.4110(7)	0.4071(2)
	$U11$	0.0764(20)	0.0636(17)	0.0220(22)	0.0788(15)
	$U22$	0.0293(15)	0.0267(13)	0.0051(13)	0.0374(11)
	$U33$	0.0638(21)	0.0574(17)	0.0939(21)	0.0841(16)
	$U12$	0.0170(15)	0.0168(12)	0.0225(13)	0.0252(10)
	$U13$	− 0.0107(16)	− 0.0075(10)	0.0198(14)	− 0.0025(11)
	$U23$	0.0121(13)	0.0134(10)	0.0270(15)	0.0173(10)
O2	x	0.5	0.5	0.5	0.5
	$U11$[b]	0.0811(21)	0.0726(16)	0.1337(34)	0.0950(14)
	$U12$[c]	− 0.0405(27)	− 0.0347(23)	− 0.0478(40)	− 0.0295(23)

[a] U(iso) was slightly negative, and therefore it was fixed at 0.000.
[b] $U11 = U22 = U33$.
[c] $U12 = U13 = U23$.

Low-Temperature Structure

The $3 \times 3 \times 3$ superstructure was evident in data obtained at − 263, 25, 45, and 66°C. Precession photographs obtained at room temperature on a small single crystal confirmed the $3 \times 3 \times 3$ superstructure. The apparent space group is $Pa\bar{3}$, which is consistent with ^{51}V NMR studies (2). Z is 108, and there are 134 positional parameters and 3490 possible peaks in the range of our data collection. A starting model was based on DLS modeling (5) as was done for isostructural SiP_2O_7 (6) and ZrP_2O_7 (7). Starting with the refined coordinates from either SiP_2O_7 or ZrP_2O_7 did not lead to a successful refinement.

Many refinements of the ZrV_2O_7 structure were conducted with DLS. Only one good structure solution was found. This was then used as a starting model for a GSAS refinement. In view of the large number of parameters,

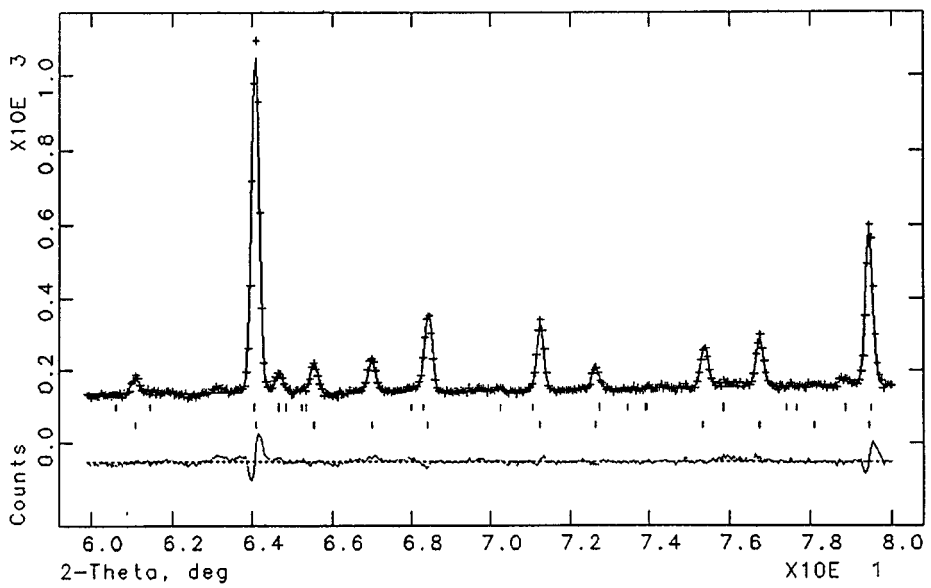

FIG. 1. Observed, calculated, and difference plots for a portion of the neutron diffraction pattern of ZrV_2O_7 at 470°C. The lower ticks are for V_2O_5.

TABLE 3
Selected Interatomic Distances (Å) and Angles (°) at Different Temperatures

	88°C	114°C	236°C	470°C
V–O1	1.637(2)	1.669(12)	1.659(4)	1.645(11)
V–O2	1.803(50)	1.734(34)	1.704(2)	1.788(40)
V–O2[a]	1.805	1.736	1.709	1.791
Zr–O1	2.066(2)	2.063(2)	2.072(4)	2.060(12)
Zr–O1–V	164.5(2)	163.8(8)	164.6(4)	164.1(7)

[a] This distance is corrected for the thermal motion of O2.

TABLE 4
Cell Parameters, Agreement Factors, and Profile Parameters for the 3×3×3 Superstructures

	−263°C	25°C	45°C	66°C
a (Å)[a]	26.2339(2)	26.3309(1)	26.3459(3)	26.3719(3)
R_{wp}	0.0788	0.0685	0.0610	0.0772
$R(F)$	0.0861	0.0679	0.0802	0.1427
$R(F^2)$	0.1040	0.0787	0.0899	0.1492
c^2	1.384	1.79	0.547	0.9132
U	45.4	40.4	67.1	40.4
V	−78.7	−72.0	−115.3	−72.03
W	132.1	132.7	144.2	132.7
A_s	15.57	15.515	14.83	15.15
F_1	−0.905	−0.302	−0.687	−0.302
F_2	−0.0543	−0.0148	−0.0632	−0.0148

[a] Standard deviation in parentheses are those calculated by GSAS. Considering the uncertainties in the wavelength and temperature, the uncertainty of the cell edges would be much larger.

some constraints were applied. All oxygen atoms of the Zr–O–V linkages (O7–O33) are constrained to the same isotropic value. Likewise all oxygen atoms of the V–O–V linkage, except those on the 3-fold axis, are constrained to the same isotropic value. Refinement results at the various temperatures are summarized in Table 4. Examples of fits between observed and calculated patterns are shown in Fig. 2. Tables 5 and 6 give the final coordinates and bond distances for the room temperature refinements.

DISCUSSION

The structure of ZrV_2O_7 is shown is Fig. 3, and a plot of cell edge vs temperature is shown for ZrV_2O_7 in Fig. 4. This is in good agreement with previous results on thermal expansion behavior above room temperature (1, 2). The point at −263°C is the first cell edge determination for ZrV_2O_7 below room temperature. This indicates that ZrV_2O_7 has positive thermal expansion from very low temperatures up to about 100°C.

We have previously attributed negative thermal expansion in ZrV_2O_7, HfV_2O_7, ZrW_2O_8, and HfW_2O_8 to transverse thermal motion of oxygen atoms in the metal–oxygen–metal linkages (2, 8). Our refinements presented here are consistent with this in the sense that the oxygen thermal motions are higher than the metal thermal motions (Table 2), and the transverse thermal motion amplitudes of oxygen are greater than those toward the metal atoms (Fig. 5). Furthermore, there appears to be a significant increase in the thermal motion of both oxygen atoms as the

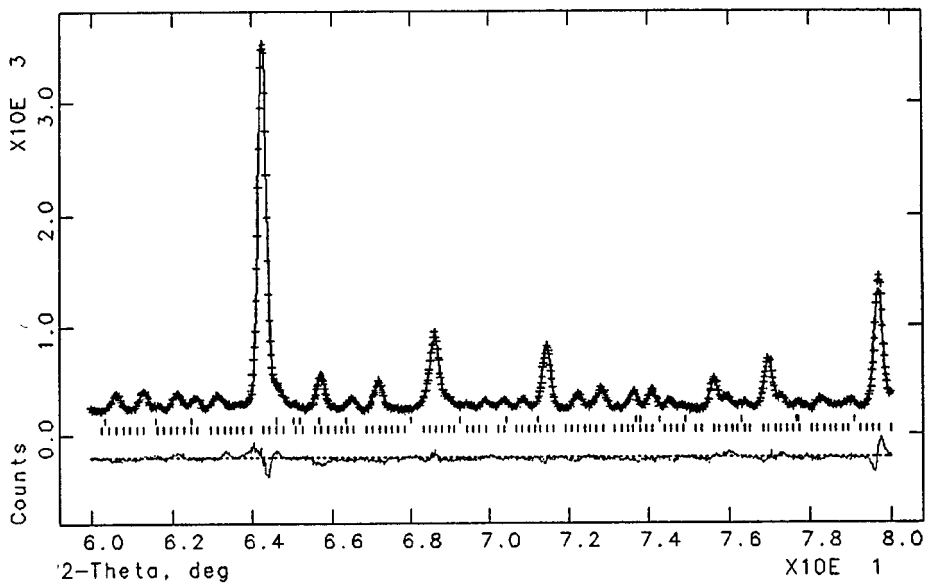

FIG. 2. Observed, calculated, and difference plots for a portion of the neutron diffraction pattern of ZrV_2O_7 at 25°C. The upper ticks are for V_2O_5.

TABLE 5
Fractional Coordinates and Thermal Parameters for ZrV_2O_7 at 25°C

Atom	x	y	z	$U \times 100$
V1	0.4635	0.1277	0.1321	0.7(5)
V2	0.4716	0.4586	0.1319	0.7(5)
V3	0.7932	0.1292	0.1331	0.7(5)
V4	0.7960	0.7961	0.1329	0.7(5)
V5	0.1299	0.4671	0.8016	0.7(5)
V6	0.1276	0.7916	0.4630	0.7(5)
V7	0.4614	0.7952	0.4639	0.7(5)
V8	0.4680	0.8014	0.7899	0.7(5)
V9	0.8001	0.8001	0.8001	0.7(5)
V10	0.4641	0.4641	0.4641	0.7(5)
V11	0.1281	0.1281	0.1281	0.7(5)
Zr1	0.3349	−0.0039	1.0002	2.24(3)
Zr2	0.3267	0.3348	−0.0005	2.24(3)
Zr3	0.9975	0.3285	0.6612	2.24(3)
Zr4	0.3361	0.6654	0.3320	2.24(3)
Zr5	0.3355	0.3355	0.3355	2.24(3)
Zr6	0.0000	0.0000	0.0000	2.24(3)
O1	0.4989	0.1541	0.1816	2.32(8)
O2	0.8347	0.1721	0.1572	2.32(8)
O3	0.5107	0.4903	0.1736	2.32(8)
O4	0.1746	0.4994	0.8347	2.32(8)
O5	0.1628	0.1628	0.1628	4.21 and −1.35[b]
O6	0.5000	0.5000	0.5000	7.74 and −3.41[b]
O7	0.1260	0.0639	0.1431	2.29(21)
O8	0.4824	0.0654	0.1283	2.29(2)
O9	0.1418	0.3992	0.1308	2.29(2)
O10	0.1599	0.0776	0.4772	2.29(2)
O11	0.4919	0.3953	0.1220	2.29(2)
O12	0.4866	0.0719	0.4696	2.29(2)
O13	0.1537	0.4090	0.4632	2.29(2)
O14	0.4623	0.4026	0.4878	2.29(2)
O15	0.8075	0.0684	0.1468	2.29(2)
O16	0.1467	0.7336	0.1393	2.29(2)
O17	0.1332	0.0653	0.7982	2.29(2)
O18	0.8157	0.7374	0.1346	2.29(2)
O19	0.8139	0.0694	0.8038	2.29(2)
O20	0.1469	0.7336	0.7960	2.29(2)
O21	0.8158	0.7426	0.8101	2.29(2)
O22	0.1414	0.4045	0.8028	2.29(2)
O23	0.1447	0.7253	0.4617	2.29(2)
O24	0.4881	0.7399	0.1291	2.29(2)
O25	0.4634	0.7300	0.4775	2.29(2)
O26	0.4754	0.4033	0.8159	2.29(2)
O27	0.4884	0.7389	0.7969	2.29(2)
O28	0.4857	0.0667	0.7889	2.29(2)
O29	0.8316	0.0740	0.4785	2.29(2)
O30	0.8089	0.4004	0.1331	2.29(2)
O31	0.8002	0.3968	0.4649	2.29(2)
O32	0.8041	0.4028	0.7997	2.29(2)
O33	0.8135	0.7272	0.4678	2.29(2)

[a] $U_{eqv} \times 100 = 4.21$ (7.74) are defined as 1/3 the trace of the diagonalized matrix. The estimated standard deviations for atomic positions from GSAS are between ±0.0005 and ±0.0008 with Zr giving the lower value.

[b] There are two values listed for O5 (and O6) since they are refined with anisotropic thermal parameters. $U11 = U22 = U33 = 0.0421$ (0.0774), and $U12 = U13 = U23 = -0.0135$ (−0.0340).

TABLE 6
Some Bond Distances (Å)[a] for ZrV_2O_7 at 25°C

V1–O1	1.75	V5–O29	1.70
V1–O8	1.72	V6–O4	1.66
V1–O9	1.71	V6–O23	1.81
V1–O10	1.71	V6–O28	1.71
V2–O3	1.72	V6–O30	1.72
V2–O11	1.77	V7–O3	1.66
V2–O12	1.74	V7–O25	1.75
V2–O13	1.75	V7–O26	1.65
V3–O2	1.70	V7–O31	1.77
V3–O15	1.68	V8–O1	1.64
V3–O16	1.63	V8–O27	1.74
V3–O17	1.79	V8–O32	1.76
V4–O2	1.71	V8–O33	1.68
V4–O18	1.63	V9–O5	1.69
V4–O19	1.75	V9–O21 × 3	1.59
V4–O20	1.68	V10–O6	1.64
V5–O4	1.69	V10–O14 × 3	1.74
V5–O22	1.68	V11–O5	1.58
V5–O24	1.71	V11–O7 × 3	1.74
Zr1–O8	2.01	Zr3–O19	1.99
Zr1–O10	2.06	Zr3–O24	2.03
Zr1–O14	2.08	Zr3–O26	2.14
Zr1–O25	2.03	Zr3–O33	2.00
Zr1–O28	2.18	Zr4–O9	2.07
Zr1–O29	2.11	Zr4–O16	2.04
Zr2–O11	2.14	Zr4–O18	2.16
Zr2–O15	2.07	Zr4–O21	2.14
Zr2–O17	2.05	Zr4–O22	2.08
Zr2–O23	2.02	Zr4–O32	2.11
Zr2–O27	2.02	Zr5–O20 × 3	2.14
Zr2–O31	2.01	Zr5–O30 × 3	2.02
Zr3–O7	2.12	Zr6–O12 × 6	2.09
Zr3–O13	2.11		

[a] Estimated standard deviations from GSAS are between ±0.02 and ±0.04 Å for V–O distances and are between ±0.02 and ±0.03 Å for Zr–O distances.

temperature is increased from 114 to 470°C (Table 2). Comparisons with the 88°C result are not meaningful because the superstructure which exists at this temperature was ignored. Comparison of the thermal motions with the 236°C result is also not possible because X-ray data were used at this temperature.

The structure of ZrV_2O_7 with the $3 \times 3 \times 3$ superstructure is not presented in detail here because a more accurate structure will soon be published based on single-crystal X-ray diffraction data. Our major conclusion is that 89% of the V–O–V bonds have bent significantly from 180°. Their average value is 160° based on our refinement and 164° based on the refinement of single-crystal X-ray data (9).

In view of the fact that ZrV_2O_7 has two phases transitions, we seriously considered the possibility that the correct space group at room temperature was of lower symmetry than $Pa\bar{3}$. Space groups $P2_13$, $R\bar{3}$, and $R3$ were investigated, but none of these gave a better fit to our neutron powder

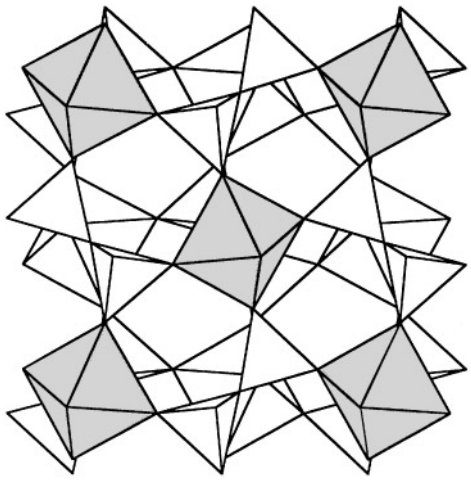

FIG. 3. Structure of ZrV_2O_7 shown as ZrO_6 octahedra and VO_4 tetrahedra.

data. Likewise, our refinement of ZrV_2O_7 from the −263°C data indicate that $Pa\bar{3}$ remains the correct space group. Another indication that the ZrV_2O_7 structure presented here is correct, although not highly accurate, comes from the result of the single-crystal X-ray refinement of ZrV_2O_7. Using the coordinates given here, that refinement converged rapidly on what was found to be the global minimum (9). Finally, our ^{51}V NMR spectrum on ZrV_2O_7 at room temperature is easily readily fit without decreasing the symmetry from $Pa\bar{3}$ (2).

It was hoped that the data collected at 88°C would indicate the nature of the intermediate phase existing between 77 and 100°C. However, the only conclusion from this study is that the superstructure is noticeably weaker in this temperature range. Our structure refinement of data collected at 88°C was therefore based on the smaller unit cell. We now know that the superstructure in this intermediate region is incommensurate (10).

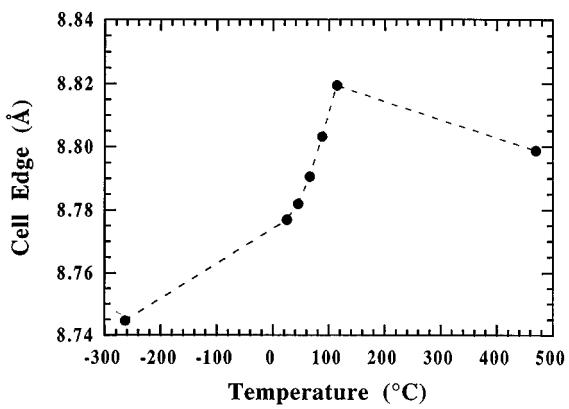

FIG. 4. Cell edge or subcell edge of ZrV_2O_7 vs temperature.

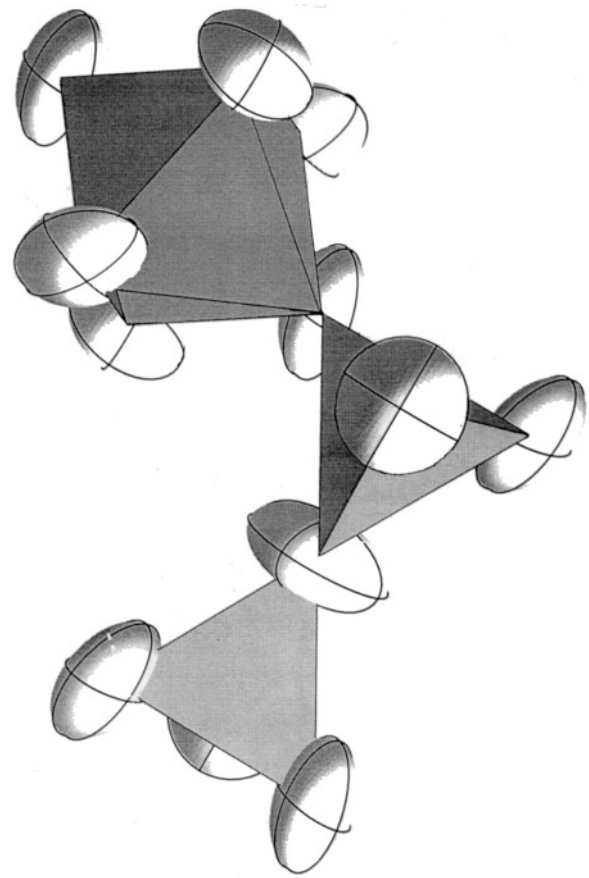

FIG. 5. Fragment of the ZrV_2O_7 structure showing thermal ellipsoids at 470°C.

The angle for the V–O–V linkage is most commonly close to 120° but apparently can range from 100 to 180°. The 180° limit is rare and is generally considered energetically unfavorable as it is also for P–O–P and Si–O–Si linkages. The thortveitite structure found for $Cd_2V_2O_7$ (11) and β-$Mn_2V_2O_7$ (12) requires that the angle of the V–O–V linkage be 180° on average. However, the oxygen atoms of this linkage in these compounds show a strong transverse displacement that can be modeled satisfactorily either as very anisotropic thermal motion or as a disordered, split atom. Diffraction studies (11, 12) have not distinguished between these two models. The same situation exists for the V–O–V linkages of ZrV_2O_7 when these linkages lie on threefold axes of either the 8.8 or 26.3 Å structure. The displacement of oxygen perpendicular to these axes may be considered as static disorder or true thermal motion. It is also possible that the best description is static disorder at lower temperatures and true thermal motion at higher temperatures.

We have previously attributed the low and negative thermal expansion in cubic AM_2O_7 compounds, as well as in ZrW_2O_8 and HfW_2O_8, to transverse thermal motions of oxygens in the metal–oxygen–metal linkages in these

structures (2, 7, 8). However, the thermal vibration of the different oxygen atoms are highly correlated with one another because the tetrahedra and octahedra have a tendency to act as rigid bodies. We have used DLS to model this correlation by investigating the flexibility of various networks, including those of zeolites, ZrV_2O_7 and ZrW_2O_8 (2, 7, 8, 13). For ZrW_2O_8 and certain zeolites such as rho and analcite, polyhedra can be rotated as rigid bodies without breaking bonds. Such rotations are not possible in the network of the ZrV_2O_7 without distorting the ZrO_6 octahedra and/or the VO_4 tetrahedra (2, 13). Using a somewhat different approach, Pryde *et al.* (14) have independently come to the same conclusion about the flexibility of the ZrV_2O_7 and ZrW_2O_8 structures. They also attribute the negative thermal expansion of ZrW_2O_8 to thermally excited rotations of rigid polyhedra, which are termed rigid unit modes or RUMs.

Because polyhedra in ZrV_2O_7 cannot undergo thermally excited rotations without changing shape, its structure has no RUMs. However, in this case, there are quasi-RUMs, that is, thermally excited polyhedra rotations that are necessarily coupled with small changes in the shapes of the polyhedra. The rigidity of polyhedra is relatively unimportant for RUMs but very important for quasi-RUMs. A major factor in enhancing the rigidity of tetrahedra and octahedra is oxygen–oxygen repulsion within these individual polyhedra. This repulsion becomes more important when the polyhedra become smaller as the central cation becomes smaller. The expected trend does appear in the cubic AM_2O_7 family, where there are quasi-RUMs but no true RUMs. As unit cell for cubic AM_2O_7 compounds increases, so does the tendency for negative thermal expansion. For TiP_2O_7 with a room-temperature subcell of 7.9 Å, normal positive thermal expansion is observed (15). For ZrP_2O_7 with a room-temperature subcell of 8.2 Å, thermal expansion above its phase transition is unusually low but positive (16). For UP_2O_7 with a at room temperature about 8.6 Å, thermal expansion is slightly negative (17, 18). For ThP_2O_7 with a at room temperature about 8.7 Å, thermal expansion has become more negative (18, 19). Finally, for ZrV_2O_7 and HfV_2O_7 with a room-temperature subcell of 8.8 Å, thermal expansion has become strongly negative above their phase transitions (1, 2). For the cubic AP_2O_7 series, the increased size of the octahedral A cation gives a less rigid octahedron and thus more facile polyhedra rotations. For ZrV_2O_7 and HfV_2O_7, the large size of VO_4 tetrahedra relative to PO_4 tetrahedra gives less rigid tetrahedra and, therefore, more facile polyhedra rotations. The low lying $3d$ orbitals of V^{5+} may also contribute to a VO_4 tetrahedra being less rigid than a PO_4 tetrahedra. The more facile rotations in turn means higher thermal motion of oxygen transverse to metal–oxygen–metal linkages, resulting in a negative thermal expansion component which may be large enough to overcome small A–O and M–O bond expansions.

ACKNOWLEDGMENTS

The furnace used to collect the high-temperature data was constructed by Richard W. Rothe, Jr. The neutron data were collected at the high-flux beam reactor at Brookhaven National Laboratory, which is supported by the Division of Materials Sciences, U.S. Department of Energy, under Contract DE-AC02-76CH0016. This work was supported in part by NSF Grant DMR-9308530.

REFERENCES

1. D. F. Craig and F. A. Hummel, *J. Am. Ceram. Soc.* **55,** 532 (1972).
2. V. Korthuis, N. Khosrovani, A. W. Sleight, N. Roberts, R. Dupree, and W. W. Warren, Jr., *Chem. Mater.* **7,** 412 (1995).
3. D. J. Buttrey, T. Vogt, U. Wildgruber, and W. R. Robinson, *J. Solid State Chem.* **111,** 118 (1994).
4. A. C. Larson and R. B. Von Dreele, "LANCE," Los Alamos National Laboratory, 1994.
5. W. M. Meier and H. Villiger, *Z. Kristallogr.* **129,** 161 (1996).
6. E. Tillmanns, W. Gebert, and W. H. Baur, *J. Solid State Chem.* **7,** 69 (1973).
7. N. Khosrovani, V. Korthuis, A. W. Sleight, and T. Vogt, *Inorg. Chem.* **35,** 485 (1996).
8. T. A. Mary, J. S. O. Evans, A. W. Sleight, and T. Vogt, *Science* **272,** 90 (1996); J. S. O. Evans, T. A. Mary, T. Vogt, M. A. Subramanian, and A. W. Sleight, *Chem. Mater.* **8,** 2809 (1996).
9. J. S. O. Evans, J. Hanson, and A. W. Sleight, in preparation.
10. R. L. Withers, J. S. O. Evans, J. Hanson, and A. W. Sleight, in preparation.
11. E. V. Sokolova, Yu. K. Egorov-Tismenko, M. A. Simonov, and T. I. Krasnenko, *Z. Kristallogr.* **31,** 1222 (1986); P. K. L. Au and C. Calvo, *Can. J. Chem.* **45,** 2297 (1967).
12. J.-H. Liao, F. Leroux, C. Payen, D. Guyomard, and Y. Piffard, *J. Solid State Chem.* **121,** 214 (1996).
13. N. Khosrovani and A. W. Sleight, *J. Solid State Chem.* **121,** 2 (1996).
14. A. K. A. Pryde, K. D. Hammonds, M. T. Dove, V. Heine, J. D. Gale, and M. C. Warren, *J. Phys. Condens. Matter* **8,** 1 (1996).
15. D. E. Harrison and F. A. Hummel, *J. Am. Ceram. Soc.* **42,** 487 (1959).
16. D. E. Harrison, H. A. McKinstry, and F. A. Hummel, *J. Am. Ceram. Soc.* **37,** 277 (1954).
17. K. M. Merz, H. T. Smyth, H. P. Kirchner, and J. L. Beal, Cornell Aeronautical Lab., Report No. PI-1273-M-8 (1960).
18. A. Burdese and M. Lucco Borlera, *Ann. Chim. Roma* **53,** 333 (1963).
19. K. R. Laud and R. A. Hummel, *J. Am. Ceram. Soc.* **54,** 296 (1971).